

Study on the relation between secondary vortex at trailing edge and motion-induced vortex vibration in heaving mode for rectangular cross sections with side ratios of $B/D=0.50-6.0$

Nade Cao*, Kazutoshi Matsuda† and Kusuo Kato**

* M. of Eng., Department of Civil Engineering and Architecture, Kyushu Institute of Technology, 1-1, Sensui-cho, Tobata-ku, Kitakyushu, Fukuoka 804-8550

† Dr. of Eng., Professor, Department of Civil Engineering and Architecture, Kyushu Institute of Technology, 1-1, Sensui-cho, Tobata-ku, Kitakyushu, Fukuoka 804-8550

** B. of Eng., Former part-time staff, Department of Civil Engineering and Architecture, Kyushu Institute of Technology, 1-1, Sensui-cho, Tobata-ku, Kitakyushu, Fukuoka 804-8550

In general, motion-induced vortex vibration is considered to be caused by the unification of separated vortex from leading edge and secondary vortex at trailing edge. However, the results of wind tunnel tests for the cross sections with side ratios of 1.18 reveal that motion-induced vortex in heaving mode might occur without the formation of secondary vortex at trailing edge. Therefore, in order to clarify the relation between secondary vortex at trailing edge and the generation of motion-induced vortex vibration, spring-supported and flow visualization tests for rectangular cross sections with side ratios of 0.50-6.0 were conducted. It was found that the stable shedding of secondary vortex at trailing edge is not necessary condition of the generation of motion-induced vortex vibration in heaving mode.

Keywords: secondary vortex at trailing edge, separated vortex from leading edge, motion-induced vortex vibration

1. INTRODUCTION

Vortex separated from rectangular cross sections can be broadly classified into Kármán vortex and motion-induced vortex (separated vortex from leading edge)¹⁾. Kármán vortex is accompanied by interference of the two separated shear layers at both the top and bottom surfaces of the structures. Motion-induced vortex is shed separately from the leading edges of the top and bottom surfaces due to the vibration of the structures. The vibration caused by the latter vortex was confirmed in past wind tunnel tests^{2), 3)} and was named either motion-induced vortex vibration^{1), 4)} or impinging-shear-layer instability⁵⁾. Motion-induced vortex vibration rarely leads to destructive damage for bluff bodies such as bridge structures. However, this vibration is prone to occur and eventually induces fatigue failure, due to the onset wind

velocity of motion-induced vortex vibration is relatively lower than divergent vibration such as galloping and torsional flutter. Therefore, in order to improve the wind-resistant performance of structures against motion-induced vortex vibration, a number of wind tunnel tests aiming to elucidate the aerodynamic characteristic of motion-induced vortex vibration have been conducted.

According to the results of conventional wind tunnel tests for rectangular cross sections with side ratios of $B/D=2-8$ (B : along-wind length, D : cross-wind length), motion-induced vortex vibration was confirmed, and its response characteristics were investigated in detail. The motion-induced vortex vibration is characterized by two types of unsteady vortices. One is the separated vortex from leading edge, while the other is generated in the wake near the trailing edge in-phase with the separated vortex from leading edge due to the vibration of the model. The latter vortex is referred to as the secondary vortex at

† Corresponding author

E-mail: matsuda@civil.kyutech.ac.jp

trailing edge¹). The separated vortex from leading edge travels on the body surface toward the trailing edge with a velocity of about 60% of the approaching flow, and reaches the trailing edge then merges with the secondary vortex at trailing edge after specific periods of vibration. Therefore, the onset reduced wind velocity of motion-induced vortex vibration depends on the side ratio of rectangular cross section, and can be expressed as:

$$V_{cr}=1/n \times 1.67B/D \quad (1)$$

in heaving mode, where $n=1, 2$ and so on¹). In general, motion-induced vortex vibration is considered to be caused by the unification of separated vortex from leading edge and secondary vortex at trailing edge¹).

In 2009, vortex-induced vibration, which occurred in relatively low wind velocity range, was confirmed in a bracing member of Ikitsuki Bridge⁶). The results of spring-supported test and unsteady lift measurement for this cross section indicate that this vortex-induced vibration is suggested to be motion-induced vortex vibration⁷). However, the side ratio of the cross section of the bracing member of Ikitsuki Bridge is $B/D=1.18$. Motion-induced vortex vibration for this kind of cross section, whose side ratio is smaller than $B/D=2.0$ was rarely confirmed by conventional wind tunnel tests. On the other hand, according to the results of flow visualization test for rectangular cross sections with side ratios of $B/D=1.18$, secondary vortex at trailing edge was not observed while motion-induced vortex vibration was generated⁸). This result shows a possibility that motion-induced vortex vibration might occur without the formation of secondary vortex at trailing edge, and indicates that the role of secondary vortex at trailing edge in motion-induced vortex vibration is not totally clear.

Therefore, in this study, rectangular cross sections with side ratios of $B/D=0.50, 0.62, 0.75, 1.0, 1.18, 2.0, 4.0, 6.0$ including side ratios smaller than $B/D=2.0$ were used as the target cross sections. Spring-supported and flow visualization tests in heaving mode were conducted in order to clarify the necessity of secondary vortex at trailing edge for the generation of motion-induced vortex vibration.

2. WIND TUNNEL TESTS

The experimental method and experimental conditions of spring-supported test and flow visualization test will be introduced in this chapter.

2.1 Spring-supported Test

In order to obtain the response characteristics of the models, especially the models with side ratios smaller than $B/D=2.0$, a spring-supported test was conducted in a closed circuit wind tunnel (cross section: 1.8m high×0.9m wide) in a smooth flow at Kyushu Institute of Technology.

Fig. 1 shows the schematic illustration of the models. **Fig. 2** shows a photograph of the section model with side ratio of $B/D=1.0$ installed in the wind tunnel.

Table 1 shows the experimental conditions for the spring-supported test. It should be noted that in the cases whose side ratios are smaller than $B/D=2$, the onset reduced wind velocity of motion-induced vortex vibration is very low. However, in order to ensure that the wind in the wind tunnel is a smooth flow, the wind velocity in the wind tunnel must be set at no less than a particular value. Thus larger models were used and the blockage ratio was moderated to 10%. With regard to this moderation of the blockage ratio, by comparing the result of $B/D=1.18$ with blockage ratio of 10% in this study with the past result of $B/D=1.18$ whose blockage ratio is 5%, it was confirmed that the difference in blockage ratio did not influence the response characteristics in the wind region of motion-induced vortex vibration⁸). Moreover, in order to ensure that the experiment can be conducted normally in both low and high reduced wind velocity regions, two different springs were used in the cases with side ratios of $B/D=0.50, 0.62$ due to the restriction of wind velocity range. The spring with a high natural frequency was used in the low reduced wind velocity region, and the spring with a low natural frequency was used in the high reduced wind velocity region. Therefore, the results of spring-supported test for the cases with side ratios of $B/D=0.50, 0.62$ were composed of both the result obtained by using the spring with high natural frequency and the result obtained by using the spring with low natural frequency. In addition, in order to get a better grasp on the response characteristic of motion-induced vortex vibration for the models with smaller side ratios, spring-supported test for the cases with side ratios of $B/D=0.50, 0.62$ were conducted in low wind velocity region again when the Scruton number was set as minimum.

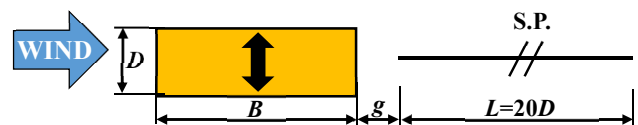


Fig. 1 Schematic illustration of the rectangular cross section model in heaving mode

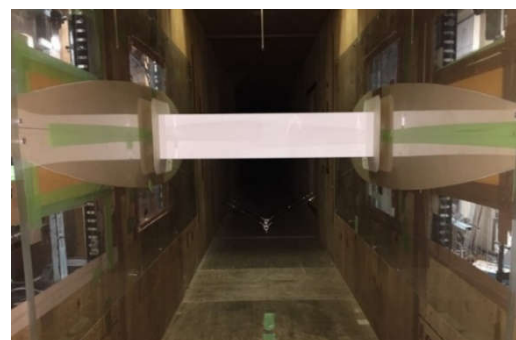


Fig. 2 Section model for spring-supported test in heaving mode ($B/D=1.0$)

Table 1 Experimental conditions of spring-supported test

B/D	B (mm)	D (mm)	Natural frequency f (Hz)	S.P.	Gap length g	Mass per unit length m (kg/m)	Logarithmic decrement of structural damping δ	Sc $=2m\delta/\rho D^2$
0.50	90	180	13.28	w/o	-	3.67	0.0065	1.2
			13.12	w/o	-	3.79	0.0083	1.6
			6.12	w/o	-	3.27	0.0097	1.6
0.62	111.6	180	10.13	w/o	-	3.69	0.0043	0.8
			10.05	w/o	-	3.82	0.0082	1.6
			6.24	w/o	-	3.14	0.0101	1.6
0.75	135	180	9.07	w/o	-	3.62	0.0086	1.6
1.0	180	180	6.70	w/o	-	3.61	0.0086	1.6
1.18	212.4	180	5.64	w/o	-	3.67	0.0085	1.6
2.0	180	90	5.22	w/o	-	5.49	0.0043	4.7
4.0	360	90	6.25	w/o	-	3.82	0.0133	10.1
			6.23	w	0.31B	3.85	0.0130	10.1
6.0	540	90	5.73	w/o	-	4.55	0.0156	14.4
			5.67	w	0.31B	4.41	0.0162	14.4

Furthermore, because the onset wind velocity of motion-induced vortex vibration and Kármán vortex-induced vibration are close to each other on the cross sections with side ratios of $B/D=2.8\sim 6.0^9$, a splitter plate (hereinafter referred as S.P.) was installed downstream of the model for the sake of weakening the influence of the Kármán vortex for the cross sections of $B/D=4.0, 6.0$. The gap length g between the model and the S.P. was set as $g=0.31B$ by referring the previous wind tunnel test⁹). The Reynolds number in the wind velocity region of motion-induced vortex vibration is $Re=9.6\times 10^3\sim 4.0\times 10^4$.

2.2 Flow Visualization Test

Flow visualization around a forced-oscillating model was conducted in a small-sized wind tunnel (cross section: 0.4m high \times 0.4m wide) at Kyushu Institute of Technology. The visualization photograph was taken by using high speed camera. **Fig. 3** shows the schematic illustration of experimental setup for flow visualization test. **Fig. 4** shows the flow field around the model in the wind tunnel. **Table 2** shows the experimental conditions of flow visualization test. The wind velocity in the wind tunnel was set as 0.6m/s or 0.8 m/s which was good for visualization. Based on the results obtained from the spring-supported test, at the onset wind velocity of motion-induced vortex vibration, the forced-oscillating amplitude was set as $2\eta/D=0.02\sim 0.34$ (every 0.01 intervals

for the cases with side ratios of $B/D=0.50\sim 1.18$, every 0.02 intervals for cases with side ratios of $B/D=2.0, 4.0, 6.0$),

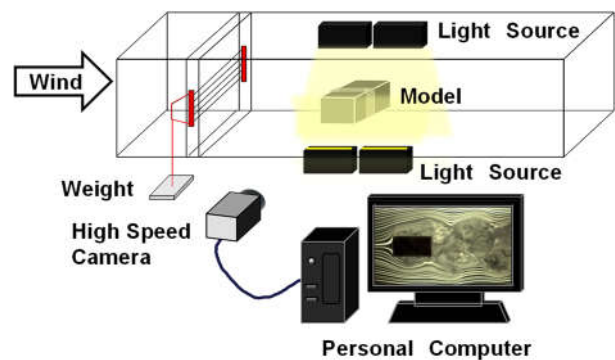


Fig. 3 Schematic illustration of experimental setup for flow visualization

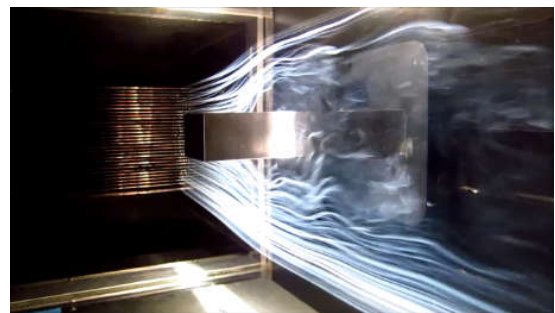


Fig. 4 Flow field around the model in small-sized wind tunnel

Table 2 Experimental conditions of flow visualization test

B/D	B (mm)	D (mm)	Wind velocity V (m/s)	Forced- oscillating frequency f (Hz)	Reduced wind velocity $V_r=V/fD$	Forced- oscillating amplitude $2\eta/D$	Reynolds number $Re=VD/\nu$
0.50	20	40	0.6	18.0	0.84	0.04-0.10	1.6×10^3
0.62	24.8	40	0.6	14.5	1.0	0.04-0.11	1.6×10^3
0.75	30	40	0.6	12.0	1.3	0.04-0.14	1.6×10^3
1.0	40	40	0.6	9.0	1.7	0.02-0.15	1.6×10^3
1.18	47.2	40	0.6	7.6	2.0	0.02-0.15	1.6×10^3
2.0	40	20	0.8	10.5	3.8	0.02-0.18	1.1×10^3
4.0	80	20	0.8	10.8	3.7	0.02-0.14	1.1×10^3
			0.8	5.6	7.1	0.02-0.34	1.1×10^3
6.0	120	20	0.8	7.7	5.2	0.02-0.18	1.1×10^3

for the sake of verifying the relation between the secondary vortex at trailing edge and the generation of motion-induced vortex vibration. The models were photographed for ten periods of vibration at their onset reduced wind velocity of motion-induced vortex vibration in each forced-oscillating amplitude.

The Reynolds number in the flow visualization test are $Re=1.1 \times 10^3$ and $Re=1.6 \times 10^3$, which are smaller than that in the spring-supported test by approximately one order of magnitude. However, the separation point in the rectangular cross section is fixed. This does not depend on the Reynolds number. Thus, it is deemed that the influence caused by different Reynolds numbers on the separated vortex from leading edge and the secondary vortex at trailing edge is small for rectangular cross sections. In addition, with regard to a rectangular cross section with a side ratio of $B/D=4$, the results of the measurement of the Strouhal number indicate that the Strouhal numbers in the Reynolds number range of $Re=1.1 \times 10^3$ - 1.6×10^3 and $Re=9.6 \times 10^3$ - 4.0×10^4 are $St=0.14$ and $St=0.13$, respectively¹⁰⁾. Then it can be considered that the influence of the difference in Reynolds number on the flow field is small. A similar tendency was also confirmed for $B/D=1$, 2¹¹⁾. Therefore, it is reasonable to have qualitative discussion based on the results of spring-supported and flow visualization tests.

3. EXPERIMENTAL RESULTS AND DISCUSSION

3.1 Response characteristic of motion-induced vortex vibration

(1) $B/D=0.50$ -1.18

The results of spring-supported test for the side ratios of $B/D=0.50$ -1.18 are shown in Figs. 5-9. Motion-induced

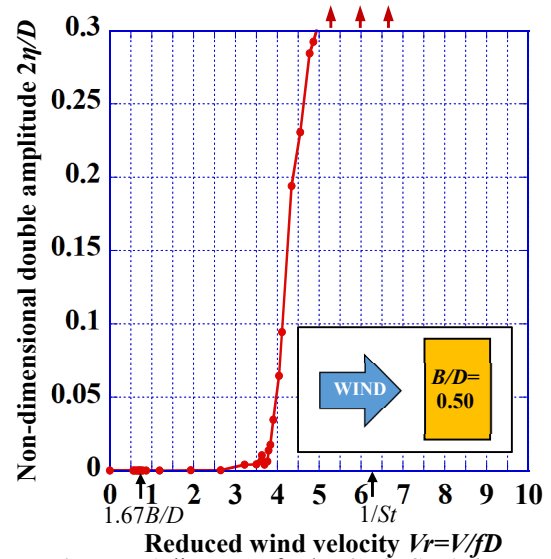


Fig. 5 V - A diagram of $B/D=0.50$, $Sc=1.6$

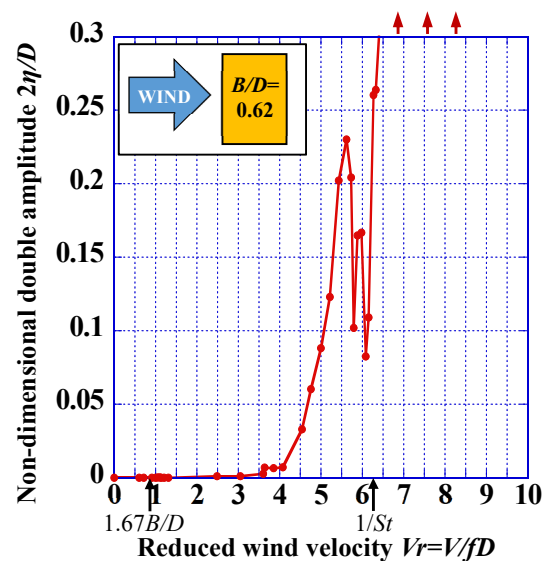


Fig. 6 V - A diagram of $B/D=0.62$, $Sc=1.6$

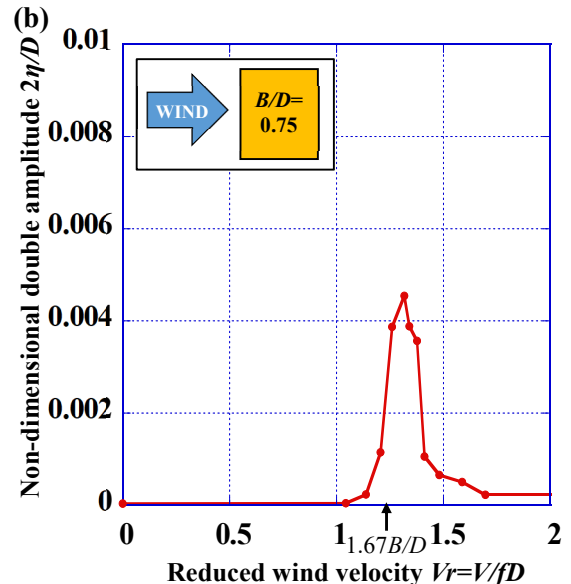
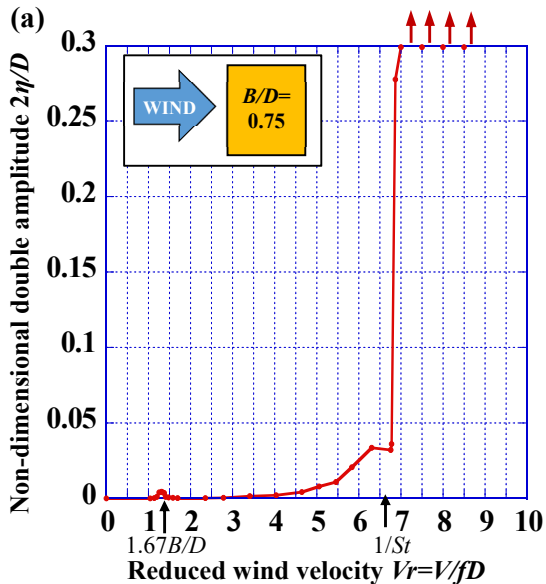


Fig. 7 (a) V - A diagram of $B/D=0.75$ and (b) enlarge view of wind velocity region of motion-induced vibration, $Sc=1.6$

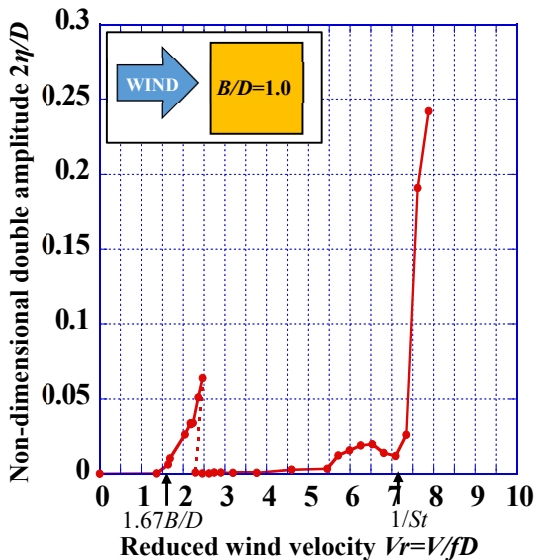


Fig. 8 V - A diagram of $B/D=1.0$, $Sc=1.6$

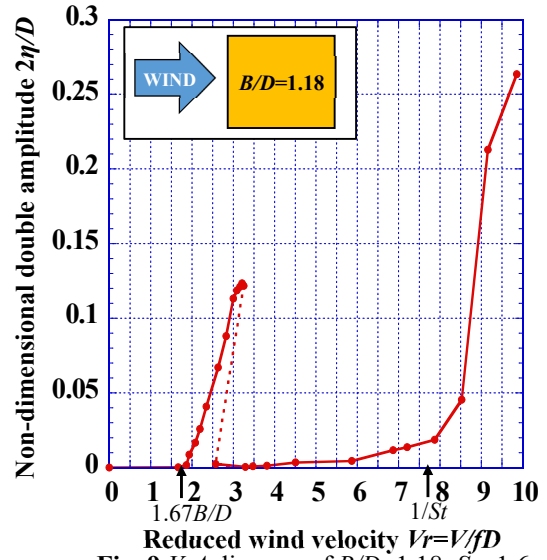


Fig. 9 V - A diagram of $B/D=1.18$, $Sc=1.6$

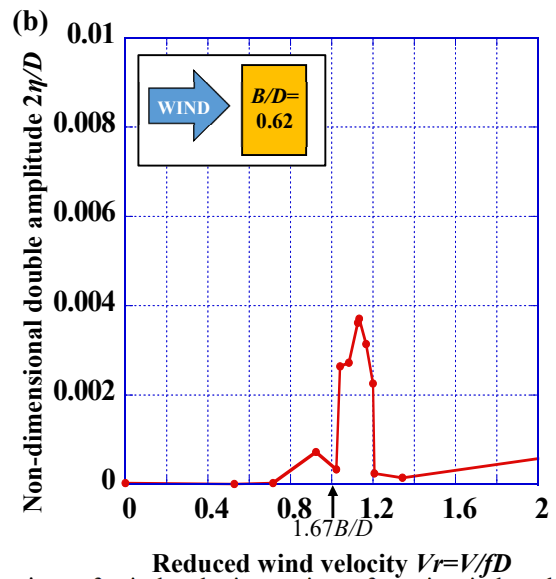
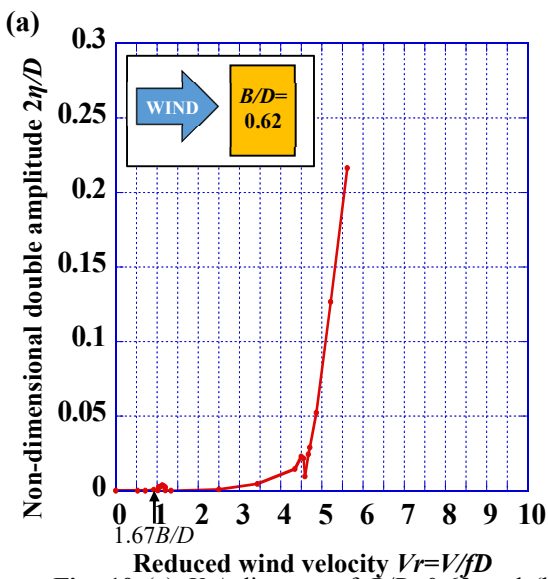


Fig. 10 (a) V - A diagram of $B/D=0.62$ and (b) enlarge view of wind velocity region of motion-induced vibration, $Sc=0.8$

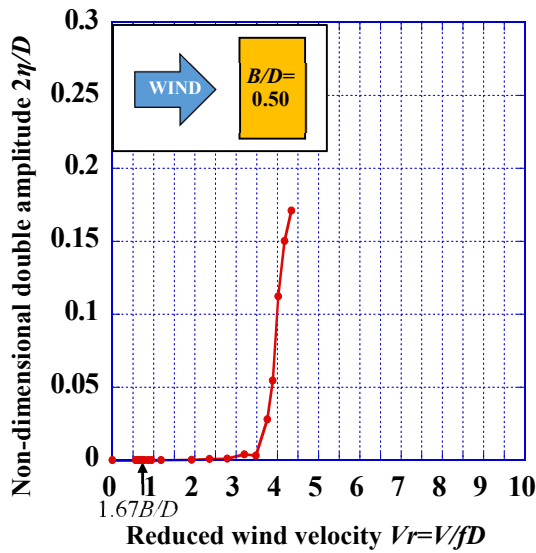


Fig. 11 V - A diagram of $B/D=0.50$, $Sc=1.2$

vortex vibration was confirmed in the cross sections of $B/D=0.75$, 1.0, 1.18 at around $V_{cr}=1.67B/D$. And it is noted that motion-induced vortex vibration was also confirmed for the cross section of $B/D=0.62$ when the Scruton number was set as 0.8, as shown in Fig. 10. With regard to the cross section of $B/D=0.50$, motion-induced vortex vibration was not confirmed, even if the Scruton number was set as 1.2, as shown in Fig. 11. By comparing these V - A diagrams, it was clear that as the side ratio B/D becomes larger, the maximum response amplitude of motion-induced vortex vibration tends to increase. The Strouhal numbers and the measurement positions for $B/D=0.50-1.18$ are shown in Table 3. The models used in the measurement of the Strouhal number are the same as the models used in spring-supported test. Fig. 12 shows the schematic illustration of the measurement position for the I-type probe. The inverse of Strouhal numbers $1/St$ was marked in the V - A diagrams for each cross section. In higher reduced wind velocity region, Kármán vortex-induced vibration was confirmed in the cross sections of $B/D=0.75$, 1.0, 1.18 in the vicinity of the inverse of Strouhal number $1/St$. However, there was an obvious discrepancy between the estimated onset wind velocity of Kármán vortex-induced vibration $1/St$ and the experimental critical wind velocity of Kármán vortex-induced vibration for the cross sections of $B/D=0.50$, 0.62. This discrepancy can be attributed to the influence of low-speed galloping¹²⁾, and was discussed in detail in our past study¹³⁾.

Table 4 shows the results of flow visualization test for the side ratios of $B/D=0.50-1.18$ at the onset wind velocity of motion-induced vortex vibration in the same forced-oscillating amplitude of $2\eta/D=0.10$. Focusing on the flow patterns of separated vortex from leading edge, it was found that in the cross sections with side ratios of $B/D=0.50$, 0.62, separated vortex from leading edge gradually separates from the upper and lower surfaces of

Table 3. St numbers for $B/D=0.50-1.18$ and the measurement positions

B/D	0.50	0.62	0.75	1.0	1.18
Vertical distance of I-type probe h	$0.6D$	$0.7D$	$0.5D$	$0.5D$	$0.4D$
Horizontal distance of I-type probe x	$2.6B$	$3.0B$	$2.0B$	$1.5B$	$1.9B$
Strouhal number St	0.16	0.16	0.15	0.14	0.13
$1/St$	6.3	6.3	6.7	7.1	7.7

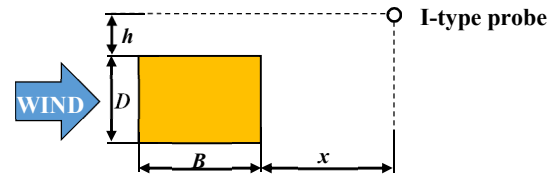


Fig. 12. Schematic illustration of the measurement position for the I-type probe

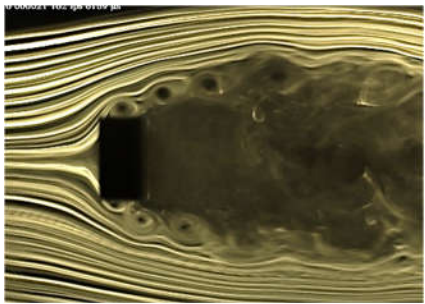
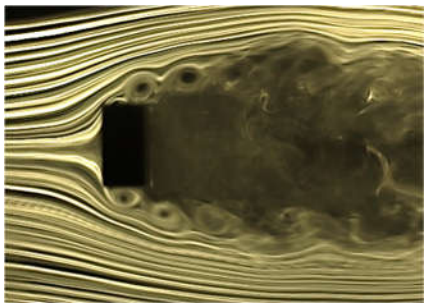
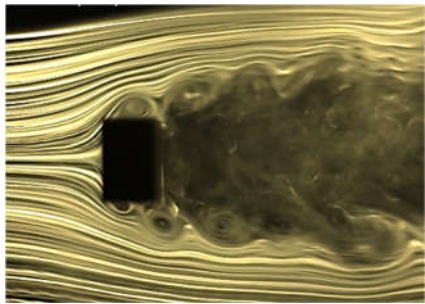
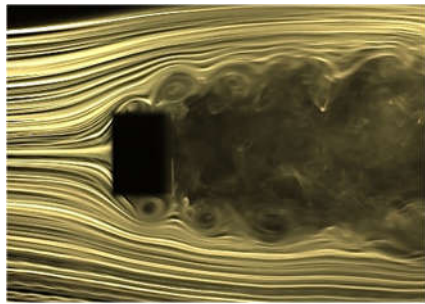
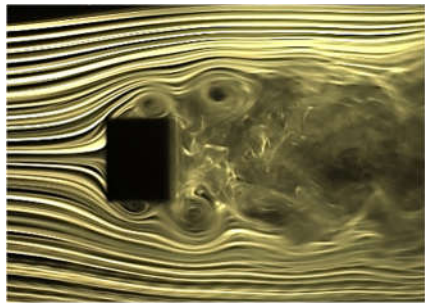
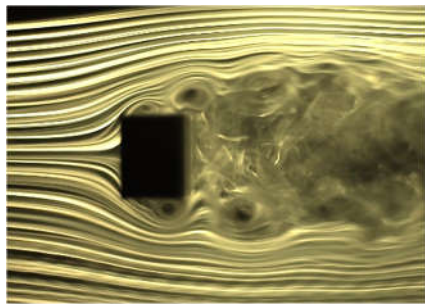
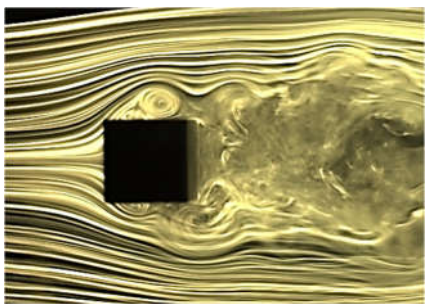
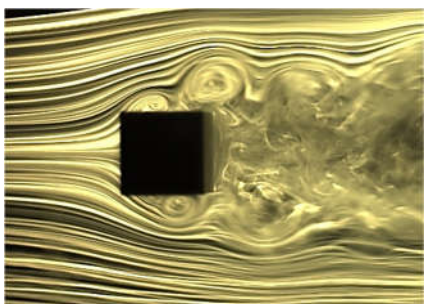
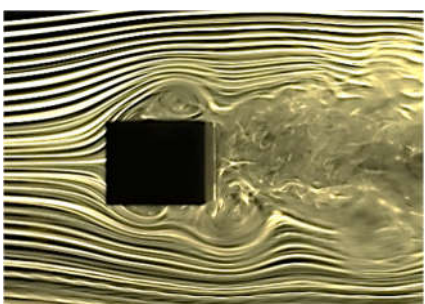
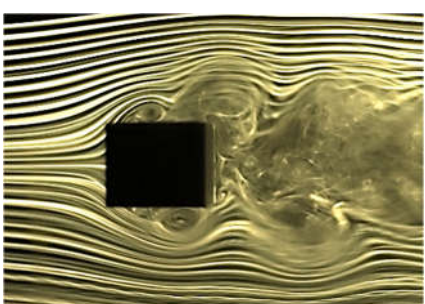
the model and flows down, instead of moving along the surfaces of the model. Thus, the fluctuating lift provided by separated vortex from leading edge did not seem to fully act on the upper and lower surfaces of the model. As the side ratio B/D becomes larger, separated vortex from leading edge tended to come closer to the model and move along the surface. Therefore, the fluctuating lift of motion-induced vortex vibration was considered to increase as the side ratio B/D became larger.

(2) $B/D=2.0$, 4.0, 6.0

The result of the spring-supported test for the case with a side ratio of $B/D=2.0$ is shown in Fig. 13. Vortex-induced vibration was confirmed to occur at approximately $Vr=3$. This vortex-induced vibration is considered to be motion-induced vortex vibration because its onset reduced wind velocity coincides with $V_{cr}=1.67B/D=3.34$. According to the previous wind tunnel test, the Strouhal number for $B/D=2.0$ is $St=0.08$ ¹⁴⁾. In the vicinity of the inverse of Strouhal number $1/St=12.5$, Kármán vortex-induced vibration was confirmed, and changed to a galloping along with the increase in wind velocity due to the small Scruton number. This result corresponds to the previous wind tunnel test¹⁵⁾.

In the cross sections of $B/D=4.0$, as shown in Fig. 14, the first vortex-induced vibration was confirmed to occur at around $Vr=3$, which roughly corresponds to the empirical value of the onset reduced wind velocity of motion-induced vortex vibration $V_{cr}=1/2 \times 1.67B/D=3.33$. This vortex-induced vibration is deemed to be motion-induced vortex vibration. The second vortex-induced vibration was confirmed to occur at approximately $Vr=7$, which is close to the inverse of the Strouhal number $1/St$

Table 4 Results of flow visualization test of $B/D=0.50-1.18$ ($2\eta/D=0.10$ for all cases)

B/D	$Vr=V/fD$	Results of flow visualization test at middle displacement with maximum upward velocity	Results of flow visualization test at middle displacement with maximum downward velocity
0.5	0.84 $=1.67B/D$		
0.62	1.0 $=1.67B/D$		
0.75	1.3 $=1.67B/D$		
1.0	1.7 $=1.67B/D$		
1.18	2.0 $=1.67B/D$		

$=7.1$ ($St=0.14$) referred from previous wind tunnel test¹⁴). It is argued that this vortex-induced vibration is not induced by the Kármán vortex, but by the motion-induced vortex, because there was no change in onset reduced wind velocity when Kármán vortex was suppressed by S.P. When S.P. was installed at $g=0.31B$, the response amplitude increased. These results have a similar tendency as the previous wind tunnel test⁹).

The results of spring-supported test for the cases with side ratios of $B/D=6.0$ are shown in Fig. 15. The Strouhal number of $B/D=6.0$ is $St=0.17$ ($1/St=5.9$), which is also referred from the previous wind tunnel test¹⁴). Motion-induced vortex vibration was confirmed to occur at approximately $Vr=5$. When S.P. was installed at $g=0.31B$, the response amplitude increased, the same as the case of $B/D=4.0$. In addition, motion-induced vortex vibration which is considered to occur at $Vcr=1.67B/D=10.0$ was not confirmed. These results also have a similar tendency as the previous wind tunnel test¹⁴).

Although the Scruton numbers in the results of spring-supported test for the side ratios of $B/D=2.0, 4.0, 6.0$ were not adjusted to the same value, according to the results of spring-supported test for the side ratios of $B/D=3.0, 4.0, 5.0$ with the same Scruton number, it is indicated that the maximum response amplitude of motion-induced vortex vibration tends to become lower as the side ratio B/D becomes larger¹⁶). In other words, the correlation between the maximum response amplitude and side ratios for the case of $B/D=2.0, 4.0, 6.0$ is contrary to that for the side ratios of $B/D=0.62-1.18$.

Table 5 shows the results of flow visualization test for the side ratios of $B/D=2.0, 4.0$ at the onset reduced wind velocity of motion-induced vortex vibration, and for $B/D=6.0$ at the reduced wind velocity of $Vcr=1.67B/D=10.0$ where motion-induced vortex is considered to occur in the same forced-oscillating amplitude of $2\eta/D=0.18$. By comparing the flow patterns of separated vortex from leading edge surrounded by a red dotted line in different cross sections, it was found that as the side ratio B/D becomes larger, separated vortex from leading edge tends to become unstable while moving toward the leeward part of the model. Especially in the case of $B/D=6.0$, separated vortex from leading edge dispersed on the middle of the upper and lower surface of the model. With regard to this property of separated vortex from leading edge, similar tendency was also obtained in the previous wind tunnel test.¹⁷) Therefore, the fluctuating lift provided by separated vortex from leading edge is considered to become weak as the side ratio B/D becomes larger. And this consideration can explain why the correlation between the maximum response amplitude of motion-induced vortex vibration and side ratio B/D for the case of $B/D=2.0, 4.0, 6.0$ is different from the case of $B/D=0.62-1.18$.

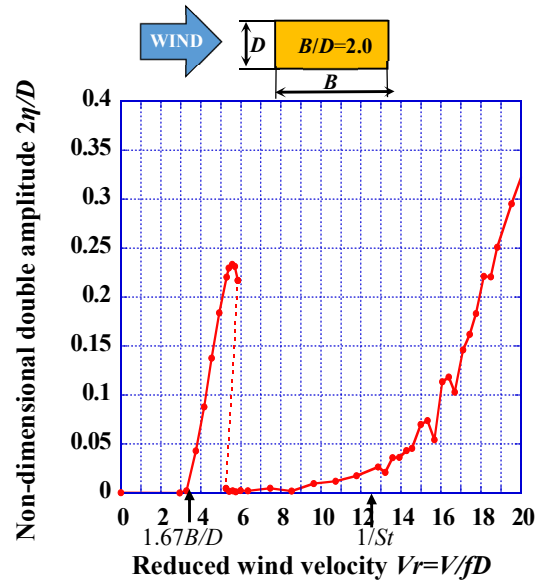


Fig. 13 V - A diagram of $B/D=2.0, Sc=4.7$

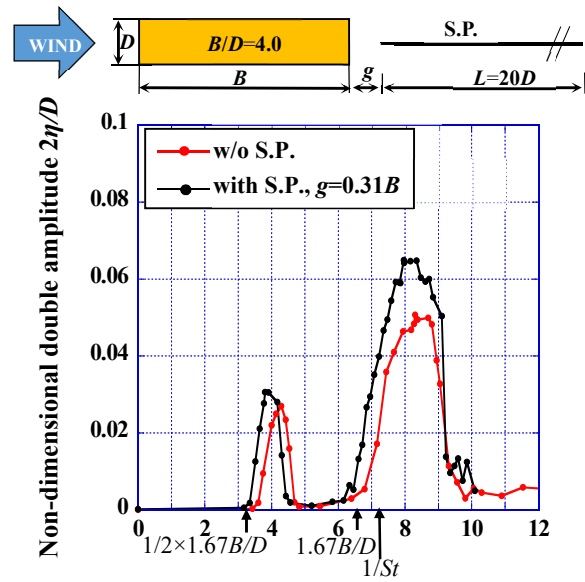


Fig. 14 V - A diagram of $B/D=4.0, Sc=10.1$

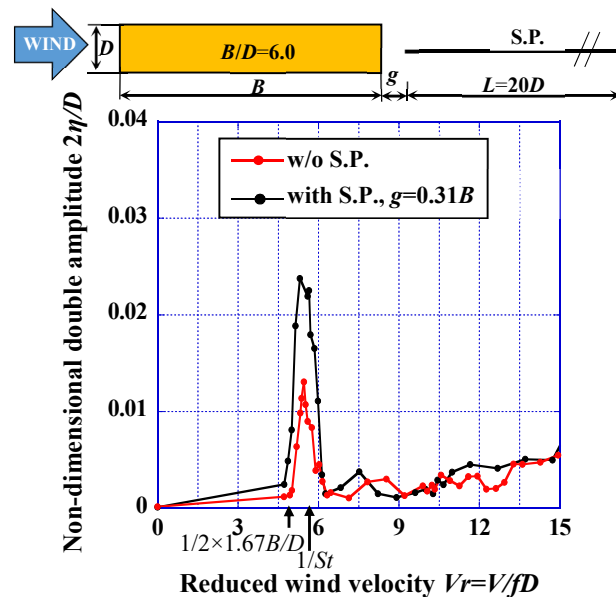
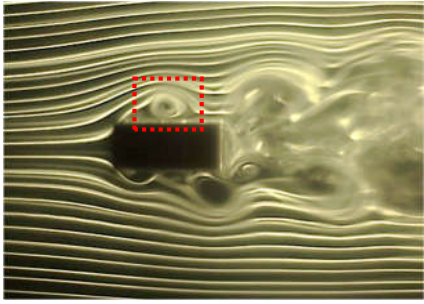
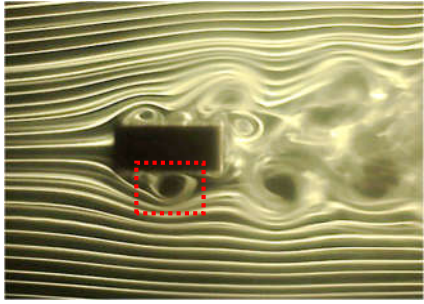
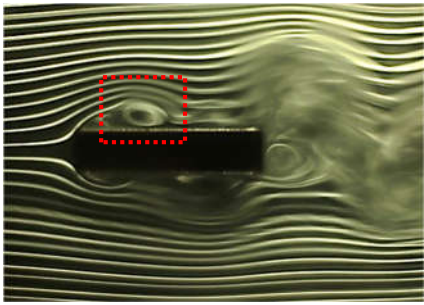
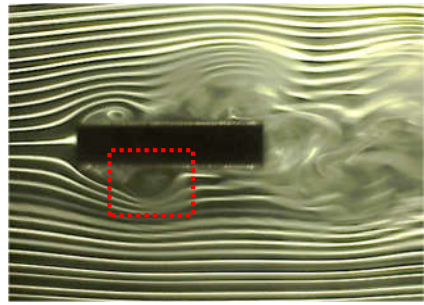
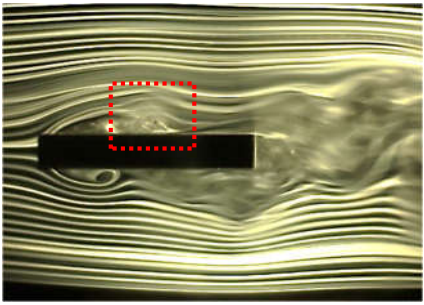
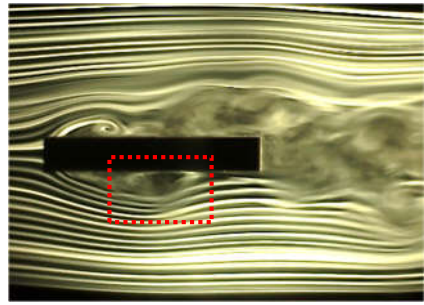


Fig. 15 V - A diagram of $B/D=6.0, Sc=14.4$

Table 5 Results of flow visualization test of $B/D=2.0, 4.0, 6.0$ ($2\eta/D=0.18$ for all cases)

B/D	$V_f=V/fD$	Results of flow visualization test at middle displacement with maximum upward velocity	Results of flow visualization test at middle displacement with maximum downward velocity
2.0	3.8 $\approx 1.67B/D$		
4.0	7.1 $\approx 1.67B/D$		
6.0	10.0 $=1.67B/D$		

3.2 The relation between secondary vortex at trailing edge and the generation of motion-induced vortex vibration

In one period of vibration, there will be up to two secondary vortices at trailing edge generated at the rear corner of the model. Therefore, when the model is forced-oscillated for ten periods, there will be up to twenty secondary vortices at trailing edge generated. Thus the generation probability of the secondary vortex at trailing edge is defined as (the number of generation times in ten periods/20) $\times 100$ (%), and it was used as an index showing the extent of stability of secondary vortex at trailing edge. **Figs. 16(a)-23(a)** show the relation between the generation probability of secondary vortex at trailing edge calculated in ten periods of vibration and forced-oscillating amplitude at the wind velocity where motion-induced vortex vibration has generated, regarding the cross sections with side ratios of $B/D=0.62-6.0$. **Figs. 16(b)-**

23(b) show the photographs of flow visualization test in higher and lower forced-oscillating amplitudes. A red dotted rectangle was added at the rear corner in the bottom surface in order to recognize whether or not the secondary vortex at trailing edge is generated. **Figs. 16(c)-23(c)** show the $V-A$ diagrams in the wind velocity region of motion-induced vortex vibration. It is noted that in the case of $B/D=0.62$, due to the high forced-oscillating frequency, flow visualization test was not conducted successfully in higher forced-oscillating amplitude where the generation probability of the secondary vortex at trailing edge can reach 100%. But it does not have influence on the discussion of the experimental results, because the main attention in this study is focused in the low forced-oscillating amplitude range.

A separated vortex from leading edge was observed in all the cross sections, regardless of the forced-oscillating amplitude. On the other hand, it was confirmed that the

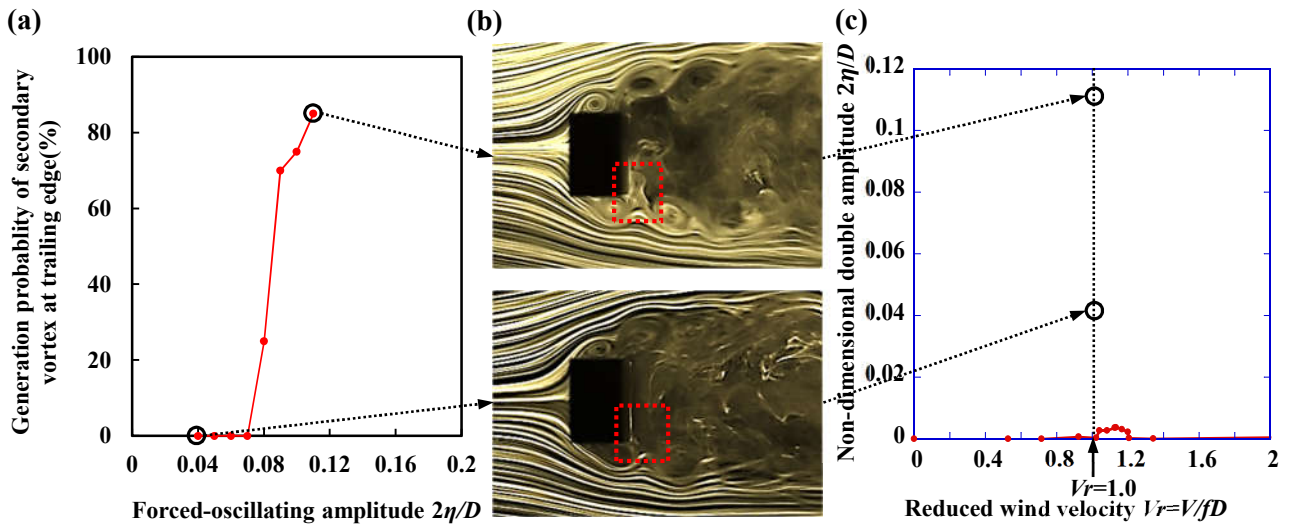


Fig. 16 (a) Generation probability for secondary vortex at the trailing edge of $B/D=0.62$ at $Vr=1.0$, (b) flow visualization result of $B/D=0.62$ at bottom displacement at $Vr=1.0$ and (c) V - A diagram of $B/D=0.62$ ($Sc=0.8$)

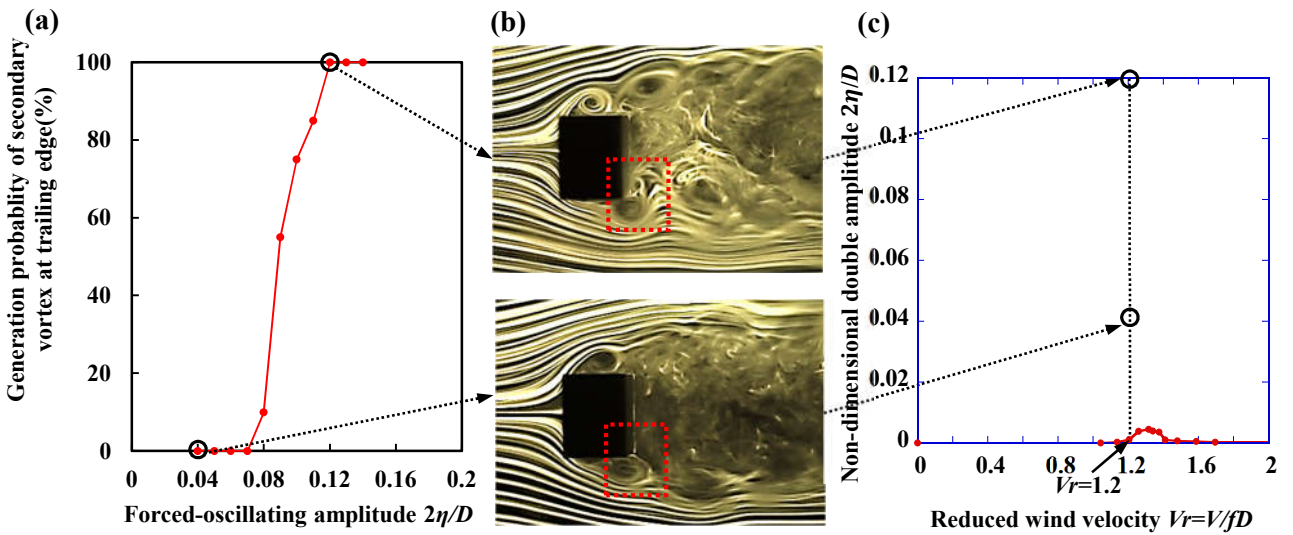


Fig. 17 (a) Generation probability for secondary vortex at the trailing edge of $B/D=0.75$ at $Vr=1.2$, (b) flow visualization result of $B/D=0.75$ at bottom displacement at $Vr=1.2$ and (c) V - A diagram of $B/D=0.75$ ($Sc=1.6$)

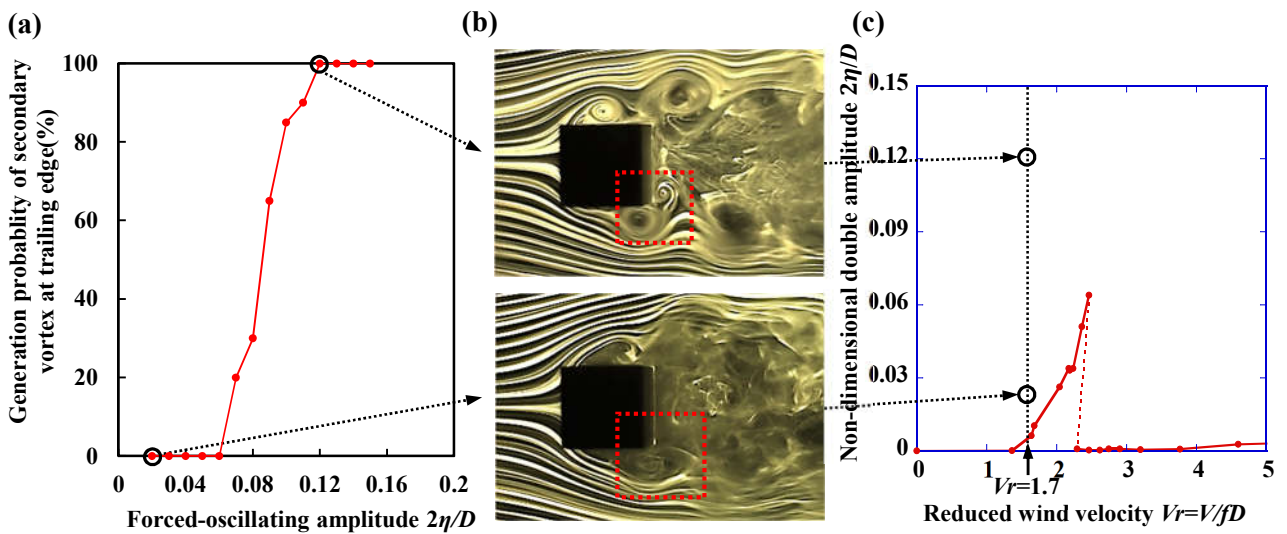


Fig. 18 (a) Generation probability for secondary vortex at the trailing edge of $B/D=1.0$ at $Vr=1.7$, (b) flow visualization result of $B/D=1.0$ at bottom displacement at $Vr=1.7$ and (c) V - A diagram of $B/D=1.0$ ($Sc=1.6$)

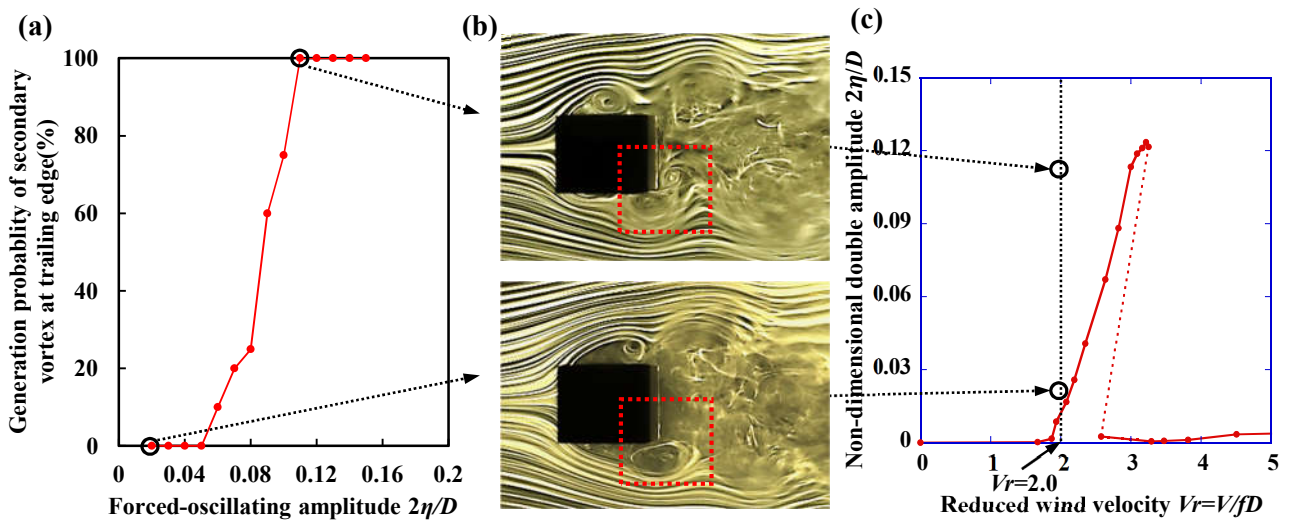


Fig. 19 (a) Generation probability for secondary vortex at the trailing edge of $B/D=1.18$ at $Vr=2.0$, (b) flow visualization result of $B/D=1.18$ at bottom displacement at $Vr=2.0$ and (c) V - A diagram of $B/D=1.18$ ($Sc=1.6$)

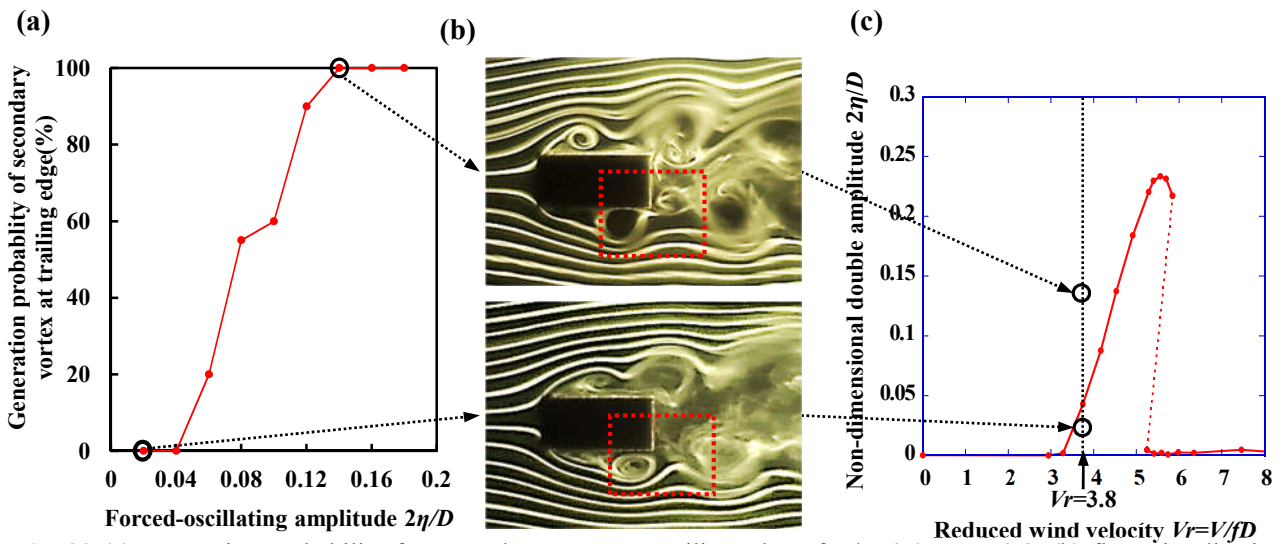


Fig. 20 (a) Generation probability for secondary vortex at trailing edge of $B/D=2.0$ at $Vr=3.8$, (b) flow visualization result of $B/D=2.0$ at bottom displacement at $Vr=3.8$ and (c) V - A diagram of $B/D=2.0$ ($Sc=4.7$)

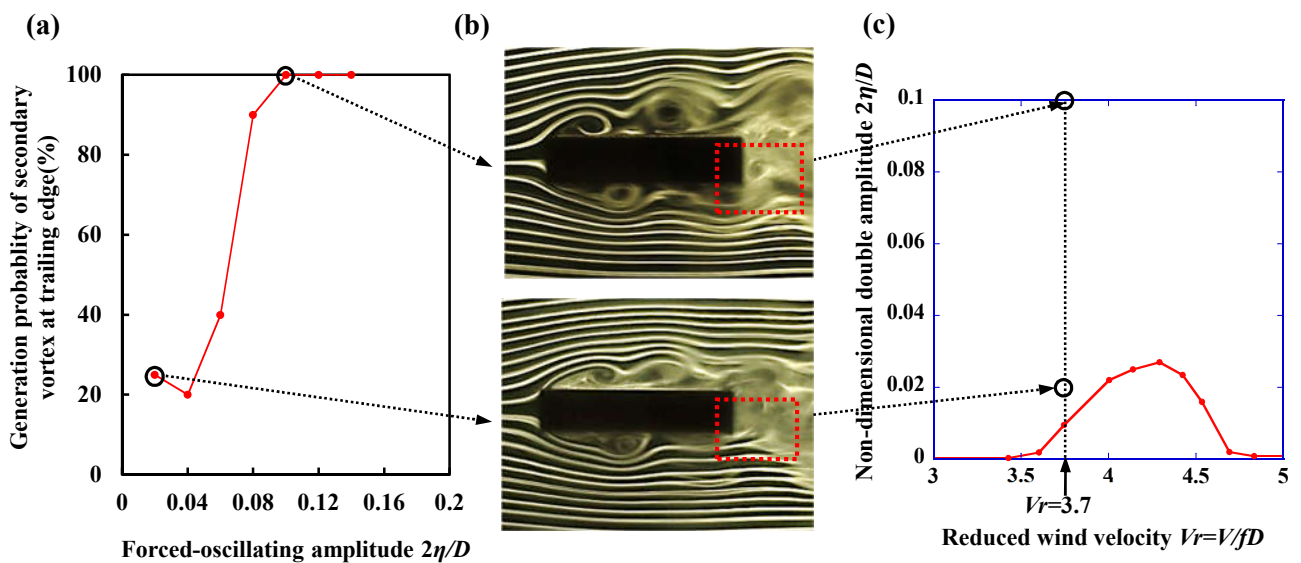


Fig. 21 (a) Generation probability for secondary vortex at trailing edge of $B/D=4.0$ at $Vr=3.7$, (b) flow visualization result of $B/D=4.0$ at bottom displacement at $Vr=3.7$ and (c) V - A diagram of $B/D=4.0$ (without S.P., $Sc=10.1$)

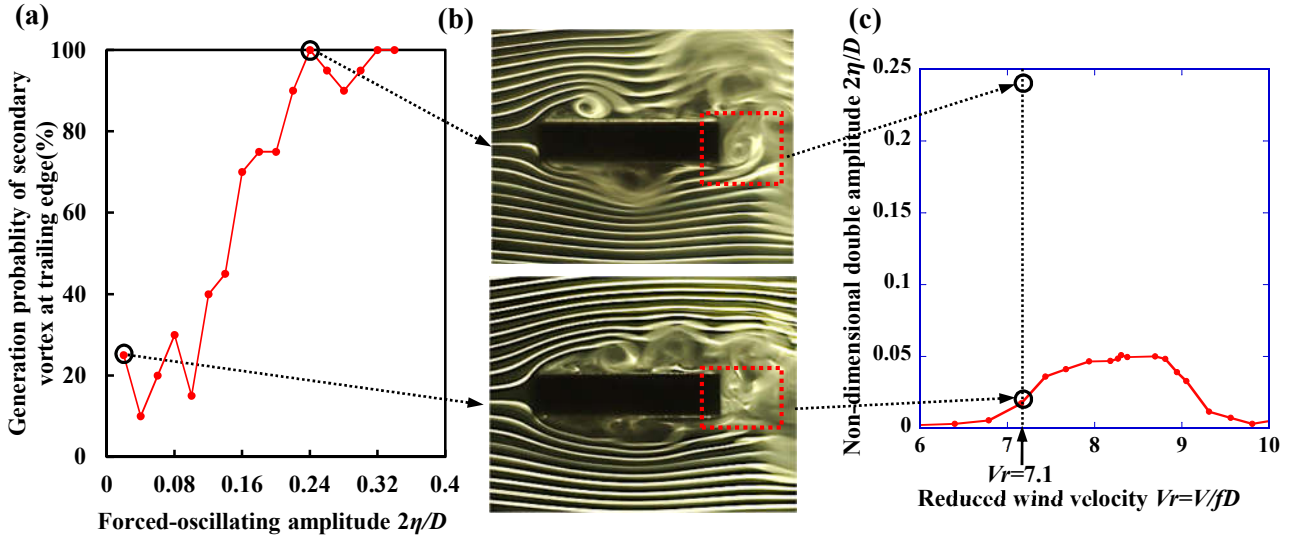


Fig. 22 (a) Generation probability for secondary vortex at trailing edge of $B/D=4.0$ at $Vr=7.1$, (b) flow visualization result of $B/D=4.0$ at bottom displacement at $Vr=7.1$ and (c) V - A diagram of $B/D=4.0$ (without S.P., $Sc=10.1$)

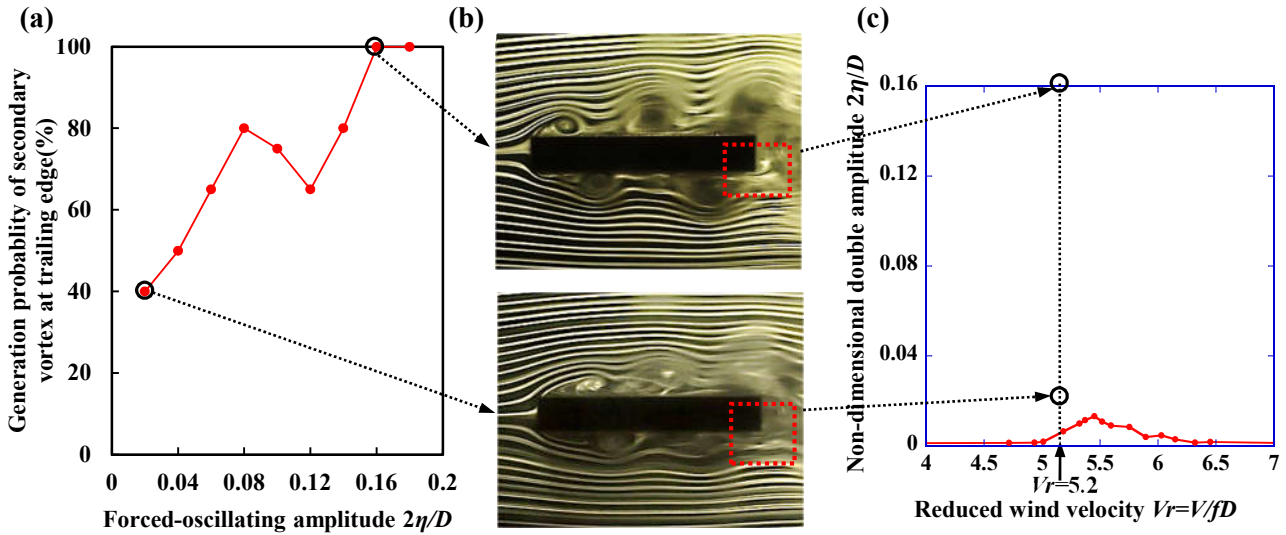


Fig. 23 (a) Generation probability for secondary vortex at trailing edge of $B/D=6.0$ at $Vr=5.2$, (b) flow visualization result of $B/D=6.0$ at bottom displacement at $Vr=5.2$ and (c) V - A diagram of $B/D=6.0$ (without S.P., $Sc=14.4$)

generation probability of secondary vortex at the trailing edge can reach 100% only in extremely high forced-oscillating amplitude, which is much higher than the response amplitude of motion-induced vortex vibration. For example, in the case of $B/D=0.75$ shown in Fig. 17, the generation probability of secondary vortex at trailing edge reached 100% in the amplitude of $2\eta/D=0.12$ at the reduced wind velocity of $Vr=1.2$. However, secondary vortex at trailing edge was not observed in amplitudes smaller than $2\eta/D=0.07$. A similar tendency was confirmed in all other cross sections, as shown in Fig.16 and Figs.18-23. At the wind velocity where motion-induced vortex vibration has been generated, in lower forced-oscillating amplitude range, the generation probability of secondary vortex at trailing edge was zero or very low. This result indicates that the shedding of secondary vortex at trailing edge is very unstable at low amplitude. In other words, motion-induced vortex vibra-

tion can occur without the stable shedding of secondary vortex at trailing edge. Therefore, it is suggested that the stable shedding of secondary vortex at trailing edge is not a necessary condition for the generation of motion-induced vortex vibration.

In addition, it should be pointed out that the relation between secondary vortex at trailing edge and motion-induced vortex vibration mentioned above is tenable only at the onset reduced wind velocity of motion-induced vortex vibration. According to the results of flow visualization test for $B/D=2.0, 4.0, 6.0$ conducted at the wind velocity where the peak response amplitude occurs, secondary vortex at trailing edge can have influence on the magnitude of exciting force of motion-induced vortex vibration at the wind velocity where the peak response amplitude occurs¹⁸).

4. CONCLUSIONS

Based on the results obtained from the spring-supported and flow visualization tests for rectangular cross sections with side ratios of $B/D=0.50, 0.62, 0.75, 1.0, 1.18, 2.0, 4.0, 6.0$ in heaving mode, the findings obtained from this research are as follows:

1. By contrasting the extents of stability of secondary vortex at trailing edge in different amplitudes at onset wind velocity of motion-induced vortex vibration, it was found that motion-induced vortex vibration can be generated without the stable shedding of secondary vortex at trailing edge. Thus it is clear that the stable shedding of secondary vortex at trailing edge is not a necessary condition for the generation of motion-induced vortex vibration. But at the wind velocity where the peak response amplitude occurs, secondary vortex at trailing edge can have influence on the magnitude of exciting force of motion-induced vortex vibration, according to our previous wind tunnel tests.
2. Motion-induced vortex vibration can be generated even on the rectangular cross sections with side ratios of $B/D=0.62, 0.75, 1.0, 1.18$, which are smaller than $B/D=2.0$. And as the side ratio B/D becomes larger, the maximum response amplitude for the side ratios of $B/D=0.62-1.18$ tends to increase. Because separated vortex from leading edge separates away from the models, instead of moving along the surface of the models for the cross section with side ratios of $B/D=0.62, 0.75$. Thus it is considered that the fluctuating lift provided by separated vortex from leading edge does not seem to fully act on the models for smaller side ratios.
3. On the other hand, for the side ratios larger than $B/D=2.0$, as the side ratio B/D becomes larger, the maximum amplitude of motion-induced vortex vibration decreases. It can be explained in a way that separated vortex from leading edge tends to become unstable while moving toward the leeward part of the model as the side ratio B/D increases. Thus the fluctuating lift provided by separated vortex from leading edge seems to decrease in a consequence.

References

- 1) Shiraishi, N. and Matsumoto, M.: On classification of vortex-induced oscillation and its application for bridge structures, *J. Wind Eng. Ind. Aerodyn.*, Vol. 14, 1-3, pp. 419-430, 1983.
- 2) Novak, M.: Galloping and vortex induced oscillations of structures, *Proc. of the 3rd Int. Conf. on Wind Effects on Buildings and Struct., Tyo*, pp. 799-809, 1971.
- 3) Otsuki, Y., Washizu, K., Tomizawa, H., Ohya, A. and Fujii, K.: Experiments on the aeroelastic instability of prismatic bars with rectangular sections, *Proc. of the 3rd Int. Conf. on Wind Effects on Buildings and Struct., Tyo*. pp. 891-898, 1971.
- 4) Komatsu, S. and Kobayashi, H: Vortex-induced oscillation of bluff cylinders, *J. Wind Eng. Ind. Aerodyn.*, Vol. 6, pp. 335-362, 1980.
- 5) Naudascher, E. and Wang, Y.: Flow-induced vibrations of prismatic bodies and grids of prisms, *J. Fluid Struct.*, Vol. 7, pp.341-373, 1993.
- 6) Nakamura, S., Shintomi, K., Tanaka, S., Nishikawa T., and Okumatsu, T.: A survey on wind conditions at the Ikitsuki Bridge, *Proc. of the 67th Annu. Meeting of JSCE*, No.67, I-323, pp.645-646, 2012. (in Japanese)
- 7) Matsuda, K., Kato, K., Hisadomi, K. and Harada, K., Low speed instability of two-dimensional rectangular prisms, *Proc. of the ASME 2013 Pressure Vessels and Piping Conf. (PVP2013)*, 97353, 2013.
- 8) Tamai, Y., Matsuda, K., Kato, K., Misawa, K. and Ikeda, I.: Experimental study on aerodynamic vibration of a bracing member with a rectangular cross section of the long-spanned truss bridge, *Proc. of the 23rd National Symp. on Wind Eng.* pp. 211-216, 2014.
- 9) Matsumoto, M., Shiraishi, N., Shirato, H., Stoyanoff, S. and Yagi, T.: Mechanism of, and turbulence effect on vortex-induced oscillations for bridge box girders, *J. Wind Eng. Ind. Aerodyn.*, Vol. 49, 1-3, pp. 467-476, 1993.
- 10) Okajima, A: Flow around a rectangular cylinder with a section of various width/height ratios, *J. of Wind Eng.*, No.17, pp. 1-19, 1983. (in Japanese)
- 11) Okajima, A: Numerical simulation of flow around rectangular cylinders, *J. Wind Eng. Ind. Aerodyn.*, Vol. 33, pp. 171-180, 1990.
- 12) Hirata, K.: Study on Galloping generation mechanism. Doctor Dissertation, Kyushu University, 1993. (in Japanese)
- 13) Matsuda, K., Kato, K., Tamai, Y., and Suda, K.: Experimental study on aerodynamic vibrations of rectangular cross sections having low side ratios, *Proc. of 8th Int. Colloquium on Bluff Body Aerodyn. and Applications, Bos.*, 2016.
- 14) Matsumoto, M., Shiraishi, N., Shirato, H., Nishizaki, T., Yamagishi, M. and Akase, M.: Vortex-induced oscillations mechanism of rectangular cylinder and effect of flow turbulence, *J. of Wind Eng.*, No. 55, pp. 65-66, 1993. (in Japanese)
- 15) Miyata, T., Miyazaki, M., Yamada, H.: Pressure distribution measurements for wind induced vibrations of box girder bridges, *J. of Wind Eng. and Industrial Aerodyn.* Vol.14, 1-3, pp. 223-234, 1983.
- 16) Shimada, K.: Evaluation of aerodynamic characteristics and aerodynamic elasticity behavior

- forecast of rectangular cylinders using $k-\varepsilon$ model, Doctor Dissertation, Kyoto University, 1999. (in Japanese)
- 17) Matsumoto, M., Yagi, T., Tamaki, H. and Tatsuki, T.: Vortex-induced vortex vibration and its effect on torsional flutter instability in the case of $B/D=4$ rectangular cylinder, *J. Wind Eng. Ind. Aerodyn.*, Vol. 96, pp. 971-983, 2008.
- 18) Matsuda, K., Kato, K., Cao, N. and Higashimura, R.: Experimental study on the effect of secondary vortices at the trailing edge on motion-induced vortex vibration, *Proc. of 15th Conf. of the Italian Association for Wind Eng., Napoli, Italy*, pp.496-506, 2018.

(Received September 20, 2019)

(Accepted February 1, 2020)